

Study of the semileptonic decay $D^0 \rightarrow \bar{K}^0 \pi^- e^+ \nu_e$



The BESIII collaboration

E-mail: besiii-publications@ihep.ac.cn

ABSTRACT: We report an improved study of the semileptonic decay $D^0 \rightarrow \bar{K}^0 \pi^- e^+ \nu_e$ based on a sample of 7.9 fb^{-1} of e^+e^- annihilation data collected at a center-of-mass energy of 3.773 GeV with the BESIII detector at the BEPCII collider. The branching fraction of this decay is measured to be $\mathcal{B}(D^0 \rightarrow \bar{K}^0 \pi^- e^+ \nu_e) = (1.444 \pm 0.022_{\text{stat}} \pm 0.024_{\text{syst}})\%$, which is the most precise to date, where the first uncertainty is statistical and the second is systematic. Based on investigation of the decay dynamics, we find that the decay is dominated by the $K^*(892)^-$ component and present an improved measurement of its branching fraction to be $\mathcal{B}(D^0 \rightarrow K^*(892)^- e^+ \nu_e) = (2.039 \pm 0.032_{\text{stat}} \pm 0.034_{\text{syst}})\%$. We also determine the ratios of the hadronic form factors for the $K^*(892)^- e^+ \nu_e$ decay to be $r_V = V(0)/A_1(0) = 1.48 \pm 0.05_{\text{stat}} \pm 0.02_{\text{syst}}$ and $r_2 = A_2(0)/A_1(0) = 0.70 \pm 0.04_{\text{stat}} \pm 0.02_{\text{syst}}$, where $V(0)$ is the vector form factor and $A_{1,2}(0)$ are the axial form factors. In addition, the $\bar{K}^0 \pi^-$ \mathcal{S} -wave component is found to account for $(5.87 \pm 0.32_{\text{stat}} \pm 0.16_{\text{syst}})\%$ of the total decay rate, corresponding to a branching fraction of $\mathcal{B}[D^0 \rightarrow (\bar{K}^0 \pi^-)_{\mathcal{S}\text{-wave}} e^+ \nu_e] = (0.085 \pm 0.005_{\text{stat}} \pm 0.003_{\text{syst}})\%$.

KEYWORDS: Charm Physics, e^+e^- Experiments

ARXIV EPRINT: [2412.10803](https://arxiv.org/abs/2412.10803)

Contents

1	Introduction	1
2	BESIII detector and Monte Carlo simulation	2
3	Event selection and data analysis	2
4	Branching fraction for $D^0 \rightarrow \bar{K}^0 \pi^- e^+ \nu_e$	4
5	Decay rate formalism for $D^0 \rightarrow \bar{K}^0 \pi^- e^+ \nu_e$	6
6	Summary	10
	The BESIII collaboration	15

1 Introduction

Studies of semileptonic (SL) decay modes of charm mesons provide valuable information on the weak and strong interactions in mesons composed of heavy quarks [1]. The SL partial decay width is related to the product of the hadronic form factor describing the strong-interaction in the initial and final hadrons, and the Cabibbo-Kobayashi-Maskawa (CKM) matrix elements $|V_{cs}|$ and $|V_{cd}|$, which parametrize the mixing between the quark flavors in the weak interaction [2]. The couplings $|V_{cs}|$ and $|V_{cd}|$ are tightly constrained by the unitarity of the CKM matrix. Hence studies of the dynamics of the SL decays allow measurements of the hadronic form factors, which are important for calibrating theoretical calculations of the relevant strong interaction effects.

The relative simplicity of theoretical description of the SL decay $D \rightarrow \bar{K} \pi e^+ \nu_e$,¹ makes it an optimal place to study the $\bar{K} \pi$ system, and to further determine the hadronic transition form factors. Measurements of $\bar{K} \pi$ resonant and non-resonant amplitudes in the decay $D^+ \rightarrow \bar{K} \pi e^+ \nu_e$ have been reported by the CLEO [3, 4], BaBar [5] and BESIII [6, 7] collaborations. In these studies, a nontrivial S -wave component is observed along with a dominant P -wave. Furthermore, the form factors in the $D \rightarrow V e^+ \nu_e$ transition, where V refers to a vector meson, have been measured in decays of $D^+ \rightarrow \bar{K}^{*0} e^+ \nu_e$ [3–6], $D^0 \rightarrow K^{*-} e^+ \nu_e$ [7], $D^{+,0} \rightarrow \rho^{+,0} e^+ \nu_e$ [8] and $D^+ \rightarrow \omega e^+ \nu_e$ [9], although the precision of these form-factor measurements is limited.

In this paper, an improved measurement of the absolute branching fraction (BF) and the form-factor parameters of the SL decay $D^0 \rightarrow \bar{K}^0 \pi^- e^+ \nu_e$ are reported. These measurements are performed using an $e^+ e^-$ annihilation data sample corresponding to an integrated luminosity of 7.9 fb^{-1} produced at $\sqrt{s} = 3.773 \text{ GeV}$ with the BEPCII collider and collected by the BESIII detector [10].

¹Throughout this paper, mesons with no explicit charge denote either a charged or neutral meson; the charge-conjugate modes are implied, unless explicitly noted.

2 BESIII detector and Monte Carlo simulation

The BESIII detector [10] records symmetric e^+e^- collisions provided by the BEPCII storage ring [11], which operates with a peak luminosity of $1 \times 10^{33} \text{ cm}^{-2} \text{ s}^{-1}$ in the center-of-mass energy range from 1.85 to 4.95 GeV. BESIII has collected large data samples in this energy region [12]. The cylindrical core of the BESIII detector covers 93% of the full solid angle and consists of a helium-based multilayer drift chamber (MDC), a plastic scintillator time-of-flight system (TOF), and a CsI(Tl) electromagnetic calorimeter (EMC), which are all enclosed in a superconducting solenoidal magnet providing a 1.0 T magnetic field. The solenoid is supported by an octagonal flux-return yoke with resistive plate counter muon identification modules interleaved with steel. The charged-particle momentum resolution at 1 GeV/ c is 0.5%, and the dE/dx resolution is 6% for electrons from Bhabha scattering. The EMC measures photon energies with a resolution of 2.5% (5%) at 1 GeV in the barrel (end cap) region. The time resolution in the TOF barrel region is 68 ps, while that in the end cap region is 110 ps. The end cap TOF system was upgraded in 2015 using multi-gap resistive plate chamber technology, providing a time resolution of 60 ps [13–15], which benefits 63% of the data used in this analysis.

Simulated data samples produced with a GEANT4-based [16] Monte Carlo (MC) package, which includes the geometric description of the BESIII detector and the detector response, are used to determine detection efficiencies and to estimate backgrounds. The simulation models the beam energy spread and initial state radiation (ISR) in the e^+e^- annihilations with the generator KKMC [17, 18]. The inclusive MC sample includes the production of $D\bar{D}$ pairs, the non- $D\bar{D}$ decays of the $\psi(3770)$, the ISR production of the J/ψ and $\psi(3686)$ states, and the continuum processes incorporated in KKMC [17, 18]. All particle decays are modelled with EVTGEN [19, 20] using branching fractions either taken from the Particle Data Group [21], when available, or otherwise estimated with LUNDCHARM [22]. Final state radiation (FSR) from charged final state particles is incorporated using the PHOTOS package [23]. The generation of signal $D^0 \rightarrow \bar{K}^0 \pi^- e^+ \nu_e$ incorporates knowledge of the form factors obtained in this work.

3 Event selection and data analysis

The analysis makes use of both “single-tag” (ST) and “double-tag” (DT) samples of D decays. The ST sample consists of \bar{D}^0 decay candidates reconstructed in one of the hadronic final states listed in table 1, which are called the tag decay modes. Within each ST sample, a subset of events is selected where the other tracks in the event are consistent with the decay $D^0 \rightarrow \bar{K}^0 \pi^- e^+ \nu_e$. This subset is referred to as the DT sample. For a specific tag mode i , the ST and DT event yields are expressed as

$$N_{\text{ST}}^i = 2N_{D^0\bar{D}^0} \mathcal{B}_{\text{ST}}^i \epsilon_{\text{ST}}^i, \quad N_{\text{DT}}^i = 2N_{D^0\bar{D}^0} \mathcal{B}_{\text{ST}}^i \mathcal{B}_{\text{SL}} \epsilon_{\text{DT}}^i,$$

where $N_{D^0\bar{D}^0}$ is the number of $D^0\bar{D}^0$ pairs, $\mathcal{B}_{\text{ST}}^i$ and \mathcal{B}_{SL} are the BFs of the \bar{D}^0 tag decay mode i and the D^0 SL decay mode, ϵ_{ST}^i is the efficiency for finding the tag candidate, and ϵ_{DT}^i is the efficiency for simultaneously finding the tag \bar{D}^0 and the SL decay. The BF for

ST mode	ΔE (GeV)	$N_{\text{ST}} (\times 10^3)$	$\epsilon_{\text{ST}} (\%)$	$\epsilon_{\text{DT}} (\%)$
$K^+\pi^-$	$[-0.027, 0.027]$	1449.3 ± 1.3	65.34 ± 0.01	6.69 ± 0.01
$K^+\pi^-\pi^-\pi^+$	$[-0.026, 0.024]$	1944.2 ± 1.6	40.83 ± 0.01	3.76 ± 0.01
$K^+\pi^-\pi^0$	$[-0.062, 0.049]$	2913.2 ± 2.0	35.59 ± 0.01	3.54 ± 0.01

Table 1. The selection requirements on ΔE , the background-subtracted ST yields, N_{ST} , in data, and the ST and DT efficiencies, ϵ_{ST} and ϵ_{DT} , for each of the three tag decay modes.

the SL decay is given by

$$\mathcal{B}_{\text{SL}} = \frac{N_{\text{DT}}}{\sum_i N_{\text{ST}}^i (\epsilon_{\text{DT}}^i / \epsilon_{\text{ST}}^i)} = \frac{N_{\text{DT}}}{N_{\text{ST}} \epsilon_{\text{SL}}}, \quad (3.1)$$

where N_{DT} is the total yield of DT events, N_{ST} is the total ST yield, and $\epsilon_{\text{SL}} = (\sum_i N_{\text{ST}}^i \times \epsilon_{\text{DT}}^i / \epsilon_{\text{ST}}^i) / \sum_i N_{\text{ST}}^i$ is the average efficiency of reconstructing the SL decay in a ST event, weighted by the measured yields of tag modes in the data.

Charged tracks are required to be well-reconstructed in the MDC detector, with the polar angle θ satisfying $|\cos\theta| < 0.93$. Their distances of the closest approach to the interaction point (IP) are required to be less than 10 cm along the beam direction and less than 1 cm in the perpendicular plane. To discriminate pions from kaons, the dE/dx and TOF information is combined to obtain particle identification (PID) likelihoods for the pion (\mathcal{L}_π) and kaon (\mathcal{L}_K) hypotheses. Pion and kaon candidates are selected using $\mathcal{L}_\pi > \mathcal{L}_K$ and $\mathcal{L}_K > \mathcal{L}_\pi$, respectively.

Photon candidates are reconstructed from isolated clusters in the EMC in the regions $|\cos\theta| \leq 0.80$ (barrel) and $0.86 \leq |\cos\theta| \leq 0.92$ (end cap). The deposited energy of a cluster is required to be larger than 25 (50) MeV in the barrel (end cap) region, and the opening angle between a shower and the nearest charged track must be at least 10° . To suppress electronic noise and energy deposits unrelated to the event, the difference between the EMC time and the event start time is required to be within $[0, 700]$ ns. To reconstruct a π^0 candidate via $\pi^0 \rightarrow \gamma\gamma$, the invariant mass of the candidate photon pair must be within $(0.115, 0.150)$ GeV/ c^2 . To improve the momentum resolution, a kinematic fit is performed to constrain the $\gamma\gamma$ invariant mass to the nominal π^0 mass [21]. The χ^2 of this kinematic fit is required to be less than 50. The fitted π^0 momentum is used for reconstruction of the \bar{D}^0 tag candidates.

The ST \bar{D}^0 decays are identified using the beam-constrained mass,

$$M_{\text{BC}} = \sqrt{(\sqrt{s}/2)^2 - |\vec{p}_{\bar{D}^0}|^2}, \quad (3.2)$$

where $\vec{p}_{\bar{D}^0}$ is the momentum of the \bar{D}^0 candidate in the rest frame of the initial e^+e^- system. To improve the purity of the tag decays, the energy difference $\Delta E = E_{\bar{D}^0} - \sqrt{s}/2$ for each candidate is required to be within approximately $\pm 3\sigma_{\Delta E}$ around the fitted ΔE peak, where $\sigma_{\Delta E}$ is the ΔE resolution and $E_{\bar{D}^0}$ is the reconstructed \bar{D}^0 energy in the initial e^+e^- rest frame. The explicit ΔE requirements for these three ST modes are listed in table 1.

The distributions of the variable M_{BC} for the three ST modes are shown in figure 1. Maximum likelihood fits to the M_{BC} distributions are performed. The signal shape is derived from the convolution of the MC-simulated signal function with a double-Gaussian function to account for resolution difference between MC simulation and data. An ARGUS

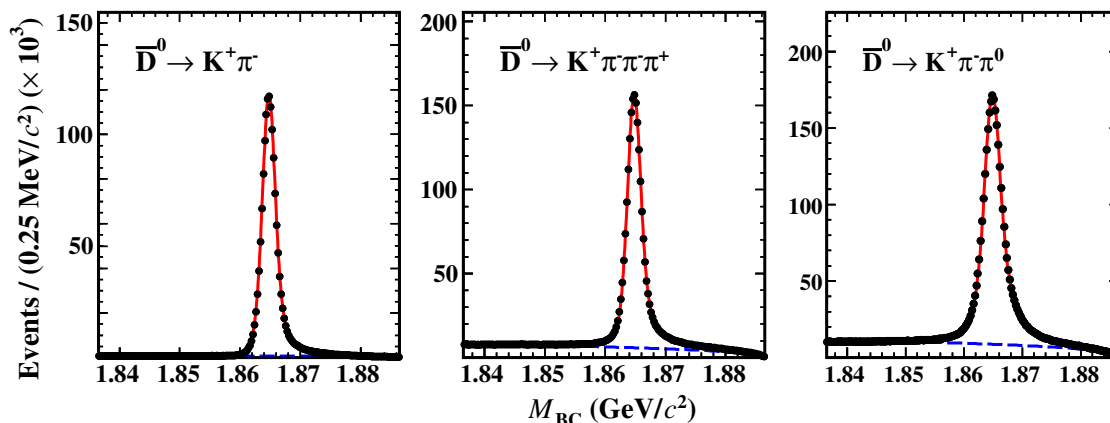


Figure 1. (Color online) The M_{BC} distributions for the three ST modes. The points are data, the solid red curves are the projection of the sum of all fit components and the dashed blue curves are the projection of the background component of the fit.

function [24] is used to describe the combinatorial background shape. For each tag mode, the ST yield is obtained by integrating the signal function over the D^0 signal region within $1.859 < M_{BC} < 1.873 \text{ GeV}/c^2$. In addition to the combinatorial background, there are also small wrong-sign (WS) peaking backgrounds in the ST \bar{D}^0 samples, from the doubly Cabibbo-suppressed decays of $\bar{D}^0 \rightarrow K^- \pi^+$, $K^- \pi^+ \pi^0$ and $K^- \pi^+ \pi^+ \pi^-$. The $\bar{D}^0 \rightarrow K_S^0 K^- \pi^+$, $K_S^0 \rightarrow \pi^+ \pi^-$ decay shares the same final state as the WS background of $\bar{D}^0 \rightarrow K^- \pi^+ \pi^+ \pi^-$. The sizes of these WS peaking backgrounds are estimated from simulation, and are subtracted from the corresponding ST yields. The background-subtracted ST yields and the ST efficiencies for three ST modes are listed in table 1. The total ST yield summed over all three ST modes is $N_{ST} = (6306.7 \pm 2.9) \times 10^3$, where the uncertainty is statistical only.

4 Branching fraction for $D^0 \rightarrow \bar{K}^0 \pi^- e^+ \nu_e$

Candidates for the SL decay $D^0 \rightarrow \bar{K}^0 \pi^- e^+ \nu_e$ are selected from the remaining tracks recoiling against the ST \bar{D}^0 mesons. The \bar{K}^0 meson is reconstructed as a $K_S^0 \rightarrow \pi^+ \pi^-$ decay, using two oppositely-charged tracks (with no PID) having an invariant mass within (0.485, 0.510) GeV/c^2 . For each K_S^0 candidate, a fit is applied to constrain the two charged tracks to a common vertex, and this K_S^0 decay vertex is required to be separated from the IP by more than twice the standard deviation of the measured flight distance. It is then required that there be only two other tracks with opposite charges in the event. The track having the same charge as the kaon on the tag side is taken as the electron candidate. For electron PID, the dE/dx and TOF measurements are combined with shower properties from the EMC to construct likelihoods for electron, pion and kaon hypotheses, \mathcal{L}'_e , \mathcal{L}'_π and \mathcal{L}'_K . The electron candidate must satisfy $\mathcal{L}'_e > 0.001$ and $\mathcal{L}'_e / (\mathcal{L}'_e + \mathcal{L}'_\pi + \mathcal{L}'_K) > 0.8$. Additionally, the EMC energy of the electron candidate has to be more than 70% of the track momentum measured in the MDC: $E/p > 0.7$. The energy loss due to bremsstrahlung is partially recovered by adding the energy of the EMC showers that are within 5° of the initial electron direction and not matched to other particles [25, 26]. The final charged track is taken as the

pion candidate and must satisfy the same PID criteria as for the ST side. The background from $D^0 \rightarrow \bar{K}^0 \pi^+ \pi^-$ decays reconstructed as $D^0 \rightarrow \bar{K}^0 \pi^- e^+ \nu_e$ is rejected by requiring the $\bar{K}^0 \pi^- e^+$ invariant mass ($M_{\bar{K}^0 \pi^- e^+}$) to be less than $1.80 \text{ GeV}/c^2$. Backgrounds containing additional π^0 mesons are suppressed by requiring the maximum energy of any unused photon ($E_{\gamma_{\max}}$) to be less than 0.25 GeV .

The energy and momentum carried by the neutrino are denoted by E_{miss} and \vec{p}_{miss} , respectively. They are calculated from the energies and momenta of the tag ($E_{\bar{D}^0}, \vec{p}_{\bar{D}^0}$) and the measured SL decay products ($E_{\text{SL}} = E_{\bar{K}^0} + E_{\pi^-} + E_{e^+}$, $\vec{p}_{\text{SL}} = \vec{p}_{\bar{K}^0} + \vec{p}_{\pi^-} + \vec{p}_{e^+}$) using the relations $E_{\text{miss}} = \sqrt{s}/2 - E_{\text{SL}}$ and $\vec{p}_{\text{miss}} = \vec{p}_{D^0} - \vec{p}_{\text{SL}}$ in the initial e^+e^- rest frame. Here, the momentum \vec{p}_{D^0} is given by $\vec{p}_{D^0} = -\hat{p}_{\text{tag}} \sqrt{(\sqrt{s}/2)^2 - m_{D^0}^2}$, where \hat{p}_{tag} is the momentum direction of the ST \bar{D}^0 and m_{D^0} is the nominal \bar{D}^0 mass [21]. Information on the undetected neutrino is obtained by using the variable U_{miss} defined by

$$U_{\text{miss}} \equiv E_{\text{miss}} - |\vec{p}_{\text{miss}}|c. \quad (4.1)$$

The U_{miss} distribution is expected to peak at zero for signal events.

Figure 2(a) shows the U_{miss} distribution of the accepted candidates for $D^0 \rightarrow \bar{K}^0 \pi^- e^+ \nu_e$ in data. To obtain the signal yield, an unbinned maximum likelihood fit to the U_{miss} distribution is performed. In the fit, the signal is described with a shape derived from the simulated signal events convolved with a Gaussian function, where the width of the Gaussian function is determined by the fit. The background is described by using the shape obtained from the MC simulation. The fitted yield of DT $D^0 \rightarrow \bar{K}^0 \pi^- e^+ \nu_e$ events is $N_{\text{DT}} = 8752 \pm 132$. The backgrounds from the non- D^0 and non- K_S^0 decays are estimated by examining the ST candidates in the M_{BC} and K_S^0 sidebands. The yield of this type of background is found to be consistent with zero and is limited to be small enough to not contribute significantly to systematic uncertainties. The DT efficiency ϵ_{DT}^i for each tag mode is summarized in the last column of table 1, and the average DT efficiency ϵ_{SL} is estimated to be $(9.79 \pm 0.01)\%$.² The difference of the K_S^0 reconstruction efficiencies between data and MC is estimated to be $-(1.8 \pm 0.6)\%$, taking into account the systematic uncertainties due to the tracking efficiencies for the charged pions, and systematic uncertainties associated with the K_S^0 mass window and decay length requirements. Hence ϵ_{SL} is corrected by -1.8% , giving $(9.61 \pm 0.01)\%$. Hence, the BF obtained is $\mathcal{B}(D^0 \rightarrow \bar{K}^0 \pi^- e^+ \nu_e) = (1.444 \pm 0.022)\%$.

Due to the DT technique, the BF measurement is insensitive to the systematic uncertainty in the ST efficiency. The uncertainty on the electron tracking efficiency (PID) is estimated to be 0.5 (0.1)% by studying a sample of $e^+e^- \rightarrow \gamma e^+e^-$ events. The uncertainty due to the pion tracking efficiency (PID) is estimated to be 0.3 (0.3)% using control samples selected from $D^0 \rightarrow K^- \pi^+ (\pi^0, \pi^+ \pi^-)$ and $D^+ \rightarrow K^- \pi^+ \pi^+ (\pi^0)$. The uncertainty from K_S^0 reconstruction is 0.6% , determined with control samples selected from $D^0 \rightarrow \bar{K}^0 \pi^+ \pi^-, \bar{K}^0 \pi^+ \pi^- \pi^0, \bar{K}^0 \pi^0$ and $D^+ \rightarrow \bar{K}^0 \pi^+, \bar{K}^0 \pi^+ \pi^0, \bar{K}^0 \pi^+ \pi^+ \pi^-$. The uncertainty associated with the $E_{\gamma_{\max}}$ requirement is estimated to be 0.2% by analyzing DT $D^0 \bar{D}^0$ events where D^0 mesons decay to hadronic final states of $D^0 \rightarrow K^- \pi^+, K^- \pi^+ \pi^0$ and $K^- \pi^+ \pi^+ \pi^-$. The uncertainty due to the modeling of the signal in simulated events is estimated to be 0.7% by varying the input form-factor

²The BFs of $K^0 \rightarrow K_S^0$ and $K_S^0 \rightarrow \pi^+ \pi^-$ are included in the detection efficiency ϵ_{DT} . The K_S^0 fraction of a K^0 is taken as 50% and the BF of $K_S^0 \rightarrow \pi^+ \pi^-$ is taken from PDG [21].

parameters determined in this work by $\pm 1\sigma$. The uncertainty associated with the fit of the U_{miss} distribution is estimated to be 1.0% by varying the fitting ranges and the shapes which parametrize the signal and background, where an asymmetric Gaussian function is used as an alternative signal function. The uncertainty associated with the fit of the M_{BC} distributions used to determine N_{ST} is 0.1% and is evaluated by varying the bin size, fit range and background distributions. Further systematic uncertainties are assigned due to the statistical precision of the simulation, 0.3%, and the input BF of the decay $K_S^0 \rightarrow \pi^+\pi^-$, 0.1%. The systematic uncertainty contributions are summed in quadrature, and the total systematic uncertainty on the BF measurement is 1.7%. Therefore, the BF of $D^0 \rightarrow \bar{K}^0\pi^-e^+\nu_e$ is determined to be $(1.444 \pm 0.022_{\text{stat}} \pm 0.024_{\text{syst}})\%$.

5 Decay rate formalism for $D^0 \rightarrow \bar{K}^0\pi^-e^+\nu_e$

The differential decay width of $D^0 \rightarrow \bar{K}^0\pi^-e^+\nu_e$ can be expressed in terms of five kinematic variables: the squared invariant mass of the $\bar{K}^0\pi^-$ system ($m_{\bar{K}^0\pi^-}^2$), the squared transfer momentum of the e^+ and ν_e (q^2), the angle between the π^- and the D^0 direction in the $\bar{K}^0\pi^-$ rest frame ($\theta_{\bar{K}^0}$), the angle between the ν_e and the D^0 direction in the $e^+\nu_e$ rest frame (θ_e), and the acoplanarity angle (χ) between the two decay planes of $\bar{K}^0\pi^-$ and $e^+\nu_e$. Neglecting the electron mass, the differential decay width of $D^0 \rightarrow \bar{K}^0\pi^-e^+\nu_e$ can be expressed as [27]

$$d^5\Gamma = \frac{G_F^2 |V_{cs}|^2}{(4\pi)^6 m_{D^0}^3} X \beta \mathcal{I}(m_{\bar{K}^0\pi^-}^2, q^2, \theta_{\bar{K}^0}, \theta_e, \chi) dm_{\bar{K}^0\pi^-}^2 dq^2 d\cos\theta_{\bar{K}^0} d\cos\theta_e d\chi, \quad (5.1)$$

where $X = p_{\bar{K}^0\pi^-} - m_{D^0}$, $\beta = 2p^*/m_{\bar{K}^0\pi^-}$, $p_{\bar{K}^0\pi^-}$ is the momentum of the $\bar{K}^0\pi^-$ system in the D^0 rest system and p^* is the momentum of \bar{K}^0 in the $\bar{K}^0\pi^-$ rest frame, and m_{D^0} is the known D^0 mass [21]. The Fermi coupling constant is denoted by G_F . The kinematic dependence of the decay density \mathcal{I} is given by

$$\begin{aligned} \mathcal{I} = & \mathcal{I}_1 + \mathcal{I}_2 \cos 2\theta_e + \mathcal{I}_3 \sin^2 \theta_e \cos 2\chi + \mathcal{I}_4 \sin 2\theta_e \cos \chi \\ & + \mathcal{I}_5 \sin \theta_e \cos \chi + \mathcal{I}_6 \cos \theta_e + \mathcal{I}_7 \sin \theta_e \sin \chi \\ & + \mathcal{I}_8 \sin 2\theta_e \sin \chi + \mathcal{I}_9 \sin^2 \theta_e \sin 2\chi, \end{aligned} \quad (5.2)$$

where $\mathcal{I}_{1,\dots,9}$ depend on $m_{\bar{K}^0\pi^-}^2$, q^2 and $\theta_{\bar{K}^0}$ and can be expressed in terms of three form factors, $\mathcal{F}_{1,2,3}$ [27]. The form factors can be expanded into partial waves including \mathcal{S} -wave (\mathcal{F}_{10}), \mathcal{P} -wave (\mathcal{F}_{i1}) and \mathcal{D} -wave (\mathcal{F}_{i2}), to show their explicit dependences on $\theta_{\bar{K}^0}$. However, the \mathcal{D} -wave component is neglected because of the limited statistics of reconstructed $D^0 \rightarrow \bar{K}^0\pi^-e^+\nu_e$. Also, no significant \mathcal{D} -wave contributions were observed for the related decay $D^+ \rightarrow K^+\pi^-e^+\nu_e$ in previous BaBar [5] and BESIII [6] analyses. Consequently, the form factors can be written as

$$\mathcal{F}_1 = \mathcal{F}_{10} + \mathcal{F}_{11} \cos \theta_{\bar{K}^0}, \mathcal{F}_2 = \frac{1}{\sqrt{2}} \mathcal{F}_{21}, \mathcal{F}_3 = \frac{1}{\sqrt{2}} \mathcal{F}_{31}, \quad (5.3)$$

where \mathcal{F}_{11} , \mathcal{F}_{21} and \mathcal{F}_{31} are related to the helicity basis form factors $H_{0,\pm}(q^2)$ by [27, 28]

$$\begin{aligned} \mathcal{F}_{11} &= 2\sqrt{2}\alpha q H_0 \mathcal{A}(m), \\ \mathcal{F}_{21} &= 2\alpha q (H_+ + H_-) \mathcal{A}(m), \\ \mathcal{F}_{31} &= 2\alpha q (H_+ - H_-) \mathcal{A}(m), \end{aligned} \quad (5.4)$$

where α is a constant factor, and $\mathcal{A}(m)$ denotes the amplitude of the \mathcal{P} -wave component, taken as the Breit-Wigner form given below in eq. (5.5). The helicity form factors can be related to the two axial-vector form factors, $A_1(q^2)$ and $A_2(q^2)$, as well as the vector form factor $V(q^2)$. The $A_{1,2}(q^2)$ and $V(q^2)$ are all taken as a one-pole form $A_{1,2}(q^2) = A_{1,2}(0)/(1 - q^2/M_A^2)$ and $V(q^2) = V(0)/(1 - q^2/M_V^2)$, with pole masses $M_V = M_{D_s^*(1-)} = 2.1121 \text{ GeV}/c^2$ [21] and $M_A = M_{D_{s1}(1+)} = 2.4595 \text{ GeV}/c^2$ [21]. The form factor $A_1(q^2)$ is common to all three helicity amplitudes. Therefore, it is natural to define two form factor ratios as $r_V = V(0)/A_1(0)$ and $r_2 = A_2(0)/A_1(0)$ at the momentum transfer square $q^2 = 0$.

The amplitude of the \mathcal{P} -wave resonance $\mathcal{A}(m)$ is expressed as [5, 6]

$$\mathcal{A}(m) = \frac{M_{K^*(892)} \Gamma_{K^*(892)}^0 (p^*/p_0^*)}{m_{K^*(892)}^2 - m_{\bar{K}^0\pi^-}^2 - i M_{K^*(892)} \Gamma(m_{\bar{K}^0\pi^-})} \frac{B(p^*)}{B(p_0^*)}, \quad (5.5)$$

where $M_{K^*(892)}$ and $\Gamma_{K^*(892)}^0$ are the pole mass and decay width of the $K^*(892)^-$ resonance, respectively. The Blatt-Weisskopf damping factor takes the form $B(p) = \frac{1}{\sqrt{1+R^2p^2}}$ with $R = 3.07 \text{ GeV}^{-1}$ [6], and $\Gamma(m_{\bar{K}^0\pi^-}) = \Gamma_{K^*(892)}^0 \left(\frac{p^*}{p_0^*}\right)^3 \frac{M_{K^*(892)}}{m_{\bar{K}^0\pi^-}} \left[\frac{B(p^*)}{B(p_0^*)}\right]^2$, where p^* is the momentum of the \bar{K}^0 in the $\bar{K}^0\pi^-$ rest frame and p_0^* is the momentum of the \bar{K}^0 at the pole mass of the $K^*(892)^-$ resonance. The parameter α given in eq. (5.4) is defined by $\alpha = \sqrt{3\pi \mathcal{B}_{K^*} / (p_0^* \Gamma_{K^*(892)}^0)}$ with $\mathcal{B}_{K^*} = \mathcal{B}(K^*(892)^- \rightarrow \bar{K}^0\pi^-) = 2/3$.

The \mathcal{S} -wave form-factor \mathcal{F}_{10} is described by [5, 6]

$$\mathcal{F}_{10} = (p_{\bar{K}^0\pi^-} m_{D^0}) \left(\frac{1}{1 - \frac{q^2}{m_A^2}} \right) \mathcal{A}_S(m), \quad (5.6)$$

where $\mathcal{A}_S(m)$ corresponds to the mass-dependent \mathcal{S} -wave amplitude. The expression $\mathcal{A}_S(m) = r_S P(m) e^{i\delta_S(m)}$ from refs. [5, 6] is adopted, in which $P(m) = 1 + x r_S^{(1)}$ with $x = \sqrt{\left(\frac{m}{m_{\bar{K}^0} + m_{\pi^-}}\right)^2 - 1}$, where r_S and $r_S^{(1)}$ are the relative intensity and the dimensionless coefficient, respectively. The \mathcal{S} -wave phase takes the form of $\delta_S(m) = \delta_{\text{BG}}^{1/2}$. The mass dependence of $\delta_{\text{BG}}^{1/2}$ is described with $\cot(\delta_{\text{BG}}^{1/2}) = 1/(a_{\text{S,BG}}^{1/2} p^*) + b_{\text{S,BG}}^{1/2} p^*/2$, where $a_{\text{S,BG}}^{1/2}$ and $b_{\text{S,BG}}^{1/2}$ are the scattering length and the effective range, respectively.

An unbinned five-dimensional maximum likelihood fit to the distributions of $m_{\bar{K}^0\pi^-}$, q^2 , $\cos\theta_{e^+}$, $\cos\theta_{\bar{K}^0}$, and χ for the $D^0 \rightarrow \bar{K}^0\pi^- e^+\nu_e$ events within $-0.05 < U_{\text{miss}} < 0.05 \text{ GeV}$ is performed in a similar manner to refs. [6, 7]. The likelihood is expressed as:

$$\mathcal{L} = \prod_{i=1}^N \text{PDF}(\xi_i, \eta) = \prod_{i=1}^N \frac{\omega(\xi_i, \eta) \epsilon(\xi_i)}{\int d\xi_i \omega(\xi_i, \eta) \epsilon(\xi_i)}, \quad (5.7)$$

where N denotes the number of the events in the fit, and $\text{PDF}(\xi, \eta)$ describes the probability density function (PDF). The argument ξ denotes the five kinematic variables characterizing the event, and η is for the parameters in the fit. The $\omega(\xi)$ and $\epsilon(\xi)$ represent the decay intensity and the acceptance of the event. Neglecting the terms independent of the fit parameters, we obtain the negative log likelihood:

$$-\ln\mathcal{L} = - \sum_{i=1}^N \ln \frac{\omega(\xi_i, \eta)}{\int d\xi_i \omega(\xi_i, \eta) \epsilon(\xi_i)}. \quad (5.8)$$

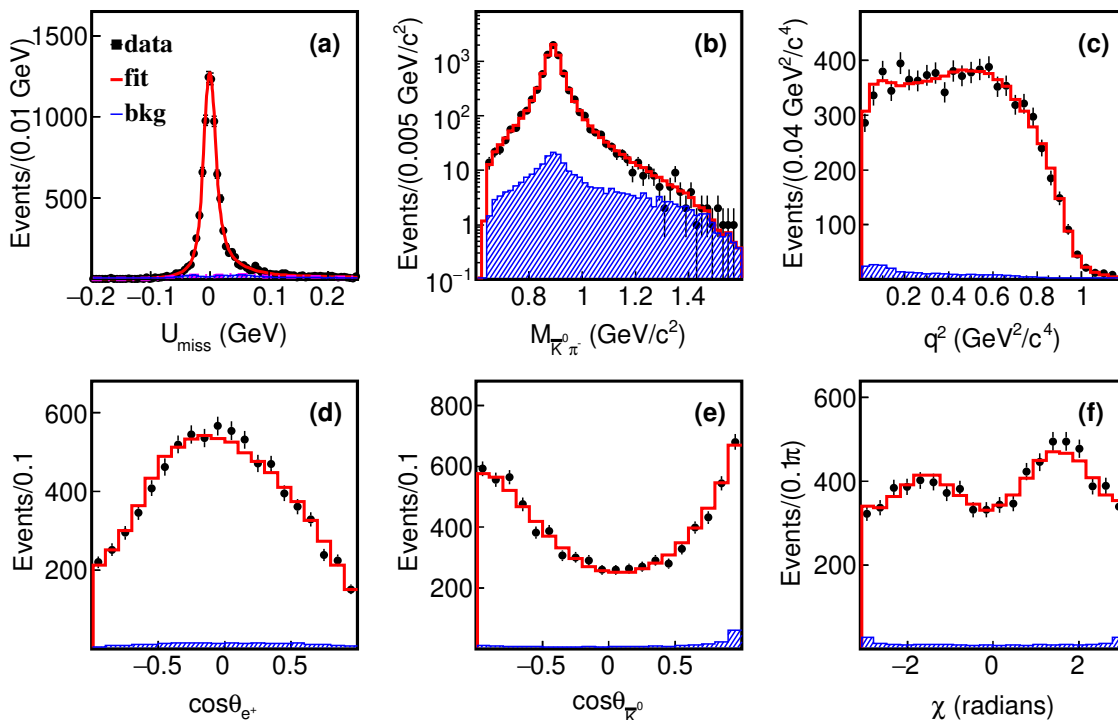


Figure 2. (Color online) (a) Fit to U_{miss} distribution of the SL candidate events. Distributions of the five kinematic variables (b) $M_{\bar{K}^0\pi^-}$, (c) q^2 , (d) $\cos\theta_{e^+}$, (e) $\cos\theta_{\bar{K}^0}$, and (f) χ for SL decay $D^0 \rightarrow \bar{K}^0\pi^-e^+\nu_e$. The dots with error bars are data, the red curves and histograms are the fit results, and the shaded histograms are the simulated background.

The acceptance efficiency is taken into account in the evaluation of $\int d\xi_i \omega(\xi_i, \eta) \epsilon(\xi_i) \propto \frac{1}{N_{\text{selected}}} \sum_{k=1}^{N_{\text{selected}}} \frac{\omega(\xi_k, \eta)}{\omega(\xi_k, \eta_0)}$, which is calculated using the signal MC events that satisfied the event selection. Here, N_{selected} refers to the number of the selected events, and η_0 denotes the set of the parameters used to produce the MC events. The resolution of each kinematic variable is examined using the signal MC events, and the central value of the resultant distribution is consistent with zero.

The projected distributions of the fit onto the fitted variables are shown in figures 2 (b–f). In this fit, the parameters r_V , r_2 , m_0 , Γ_0 , r_S , $a_{S,\text{BG}}^{1/2}$ and $r_S^{(1)}$ are free, while $b_{S,\text{BG}}^{1/2}$ is fixed to $-0.81 \text{ (GeV}/c)^{-1}$, based on the analysis of $D^+ \rightarrow K^+\pi^-e^+\nu_e$ at BESIII [6]. The fit results are summarized in table 2. The goodness of fit is estimated by using the χ^2/ndof , where ndof denotes the number of degrees of freedom. The χ^2 is calculated from the comparison between the measured and expected number of events in the five-dimensional space of the kinematic variables $m_{\bar{K}^0\pi^-}$, q^2 , $\cos\theta_{e^+}$, $\cos\theta_{\bar{K}^0}$, and χ which are divided into 2, 2, 3, 3, and 3 bins, respectively. The bins are set with different sizes, so that they contain sufficient numbers of signal events for credible χ^2 calculation. The χ^2 value is calculated as

$$\chi^2 = \sum_i^{N_{\text{bin}}} \frac{(n_i^{\text{data}} - n_i^{\text{fit}})^2}{n_i^{\text{data}}}, \quad (5.9)$$

Variable	Value
$M_{K^*(892)^-}$ (MeV/c ²)	$892.3 \pm 0.5 \pm 0.2$
$\Gamma_{K^*(892)^-}$ (MeV)	$46.5 \pm 0.8 \pm 0.2$
r_S (GeV) ⁻¹	$-13.36 \pm 0.93 \pm 0.49$
$a_{S,BG}^{1/2}$ (GeV/c) ⁻¹	$3.31 \pm 0.23 \pm 0.34$
$r_S^{(1)}$	$-0.04 \pm 0.06 \pm 0.03$
r_V	$1.48 \pm 0.05 \pm 0.02$
r_2	$0.70 \pm 0.04 \pm 0.02$

Table 2. The fit results, where the first uncertainties are statistical and the second are systematic.

where N_{bin} is the number of bins, n_i^{data} denotes the measured number of events of the i -th bin, and n_i^{fit} denotes the expected number of events of the i th bin. The ndof is defined as the number of bins minus the number of fit parameters. The χ^2/ndof obtained is 113.7/101. The fit procedure is validated using a large simulated sample of inclusive events, where the pull distribution of each fitted parameter is found to be consistent with a normal distribution.

The fit fraction of each component can be determined by the ratio of the decay intensity of the specific component to that of the total intensity. The fractions of \mathcal{S} -wave and \mathcal{P} -wave ($K^*(892)^-$) are $f_{S\text{-wave}} = (5.87 \pm 0.32(\text{stat}))\%$ and $f_{K^*(892)^-} = (94.15 \pm 0.32(\text{stat}))\%$, respectively, where the uncertainty propagation includes correlations among the underlying parameters.

The systematic uncertainties of the fitted parameters and the fractions of S -wave and $K^*(892)^-$ components are defined as the difference between the fit results in nominal conditions and those obtained with varied conditions. The systematic uncertainties due to the $E_{\gamma \text{max}}$, $M_{\bar{K}^0\pi^-e^+}$ and E/p requirements are estimated by using alternative requirements of $E_{\gamma \text{max}} < 0.20$ GeV, $M_{\bar{K}^0\pi^-e^+} < 1.75$ GeV/c² and $E/p > 0.75$, respectively. The systematic uncertainty due to the background fraction is estimated by varying its value by $\pm 10\%$ which accounts for the possible difference of the background fraction in the selected U_{miss} region. The systematic uncertainties arising from the tracking and PID placed on the charged pion, the electron and the K_S^0 are estimated by varying the pion and electron tracking and PID efficiencies, and K_S^0 detection efficiency by $\pm 0.5\%$, $\pm 0.5\%$ and $\pm 0.6\%$, respectively. The systematic uncertainty due to neglecting a possible contribution from the D -wave component is estimated by incorporating the D -wave component in eq. (5.3). The systematic uncertainty in the fixed parameter $b_{S,BG}^{1/2}$ is estimated by varying its nominal values by $\pm 1\sigma$. All of the variations mentioned above will result in differences of the fitted parameters and the extracted fractions of \mathcal{S} -wave and $K^*(892)^-$ components from that under the nominal conditions. These differences are assigned as the systematic uncertainties and summarized in table 3, where the total systematic uncertainty is obtained by adding all contributions in quadrature.

Parameter	$E_{\gamma \max}$	$M_{\bar{K}^0\pi^-e^+}$	E/p	f	Tracking, PID	D -wave	$b_{S,BG}^{1/2}$	Total
$M_{K^*(892)^-}$	0.01	0.01	0.01	0.00	0.01	0.01	0.01	0.02
$\Gamma_{K^*(892)^-}$	0.36	0.17	0.30	0.11	0.37	0.15	0.44	0.78
r_S	0.47	1.16	2.37	1.30	1.26	1.74	0.01	3.67
$a_{S,BG}^{1/2}$	0.12	0.95	0.27	0.29	0.28	3.01	10.0	10.5
$r_S^{(1)}$	17.4	26.8	46.0	43.4	18.6	17.1	17.7	77.3
r_V	0.17	0.97	0.66	0.14	0.69	0.14	0.22	1.40
r_2	0.70	0.95	1.92	0.21	0.07	0.01	2.59	3.44
$f_{K^*(892)^-}$	0.05	0.04	0.01	0.08	0.07	0.08	0.06	0.17
$f_{S\text{-wave}}$	0.85	0.68	0.17	1.36	1.19	1.36	0.85	2.66

Table 3. Systematic uncertainties on the fitted parameters, in %.

6 Summary

In summary, using 7.9 fb^{-1} of e^+e^- annihilation data collected at $\sqrt{s} = 3.773 \text{ GeV}$ by the BESIII detector, the absolute BF of $D^0 \rightarrow \bar{K}^0\pi^-e^+\nu_e$ is measured to be $\mathcal{B}(D^0 \rightarrow \bar{K}^0\pi^-e^+\nu_e) = (1.444 \pm 0.022_{\text{stat}} \pm 0.024_{\text{syst}})\%$, which presents the most precise measurements to date [21]. By analyzing the dynamics of $D^0 \rightarrow \bar{K}^0\pi^-e^+\nu_e$ decay, the \mathcal{S} -wave component is measured with a fraction $f_{S\text{-wave}} = (5.87 \pm 0.32_{\text{stat}} \pm 0.16_{\text{syst}})\%$, leading to $\mathcal{B}[D^0 \rightarrow (\bar{K}^0\pi^-)_{S\text{-wave}}e^+\nu_e] = (0.085 \pm 0.005_{\text{stat}} \pm 0.003_{\text{syst}})\%$. The \mathcal{P} -wave component is observed with a fraction of $f_{K^*(892)^-} = (94.15 \pm 0.32_{\text{stat}} \pm 0.16_{\text{syst}})\%$ and the corresponding BF is given as $\mathcal{B}(D^0 \rightarrow K^*(892)^-e^+\nu_e) = (2.039 \pm 0.032_{\text{stat}} \pm 0.034_{\text{syst}})\%$ with $\mathcal{B}(K^*(892)^- \rightarrow \bar{K}^0\pi^-) = 2/3$. In addition, the form factor ratios of the $D^0 \rightarrow K^*(892)^-e^+\nu_e$ decay are determined to be $r_V = 1.48 \pm 0.05_{\text{stat}} \pm 0.02_{\text{syst}}$ and $r_2 = 0.70 \pm 0.04_{\text{stat}} \pm 0.02_{\text{syst}}$. The reported results in this work are consistent with, and more precise than the previous measurements and hence supersede results reported in ref. [7]. The difference of $a_{S,BG}^{1/2}$ between this work and that reported in ref. [7] are mainly introduced by the different parameterization of the \mathcal{S} -wave phase.³ The comparisons of the measured BF and form-factor parameters between this measurement and theoretical calculations are shown in table 4 and figure 3. At a confidence level of 95%, our measured BF disfavors the central values in refs. [29, 33, 34], and the measured r_2 disfavors the central values in refs. [30, 32, 35]. Note that unlike ref. [7], the parameter $r_S^{(1)}$ is now free in the fit, giving a more general parameterization for the \mathcal{S} -wave component in the present work. This affects the comparison of uncertainties on the r_V and r_2 parameters in the table 4, where the PDG results are dominated by ref. [7].

The value of $A_1(0)$ can be obtained by integrating eq. (5.1), restricted to $K^*(892)^-$ contribution, over the three angles:

$$\frac{d^2\Gamma}{dq^2 dm^2} = \frac{2}{9} \frac{G_F^2 |V_{cs}|^2}{(4\pi)^5 m_{D^0}^2} p_{\bar{K}^0\pi} \beta (|\mathcal{F}_{11}|^2 + |\mathcal{F}_{21}|^2 + |\mathcal{F}_{31}|^2). \quad (6.1)$$

³In ref. [7], the \mathcal{S} -wave phase takes the form of $\delta_S(m) = \delta_{BG}^{1/2} + \delta_{\bar{K}_0^*(1430)}$ instead of $\delta_S(m) = \delta_{BG}^{1/2}$ described in the paper.

	$\mathcal{B}_{D^0 \rightarrow K^*(892)^- e^+ \nu_e}$ (%)	r_V	r_2	$A_1(0)$
This work	$2.039 \pm 0.032 \pm 0.034$	$1.48 \pm 0.05 \pm 0.02$	$0.70 \pm 0.04 \pm 0.02$	$0.610 \pm 0.007 \pm 0.004$
CQM [29]	2.46	1.56	0.74	0.66
HM χ T [30]	2.20	1.60	0.50	0.62
LCSR [31]	2.12 ± 0.09	$1.39^{+0.06}_{-0.07}$	$0.60^{+0.06}_{-0.07}$	$0.571^{+0.020}_{-0.022}$
CLFQM [32, 33]	3.0 ± 0.3	1.36 ± 0.04	0.83 ± 0.02	0.72 ± 0.01
CCQM [34]	2.96	1.22 ± 0.24	0.92 ± 0.18	0.74 ± 0.11
RQM [35]	1.92	1.53	0.85	0.608
hQCD [36]	–	1.40	0.63	0.631
PDG 2024 [21]	2.15 ± 0.16	1.46 ± 0.07	0.68 ± 0.06	–

Table 4. Comparisons of the measured BF and form-factor parameters for $D^0 \rightarrow K^*(892)^- e^+ \nu_e$, with various theoretical calculations and PDG averaged results.

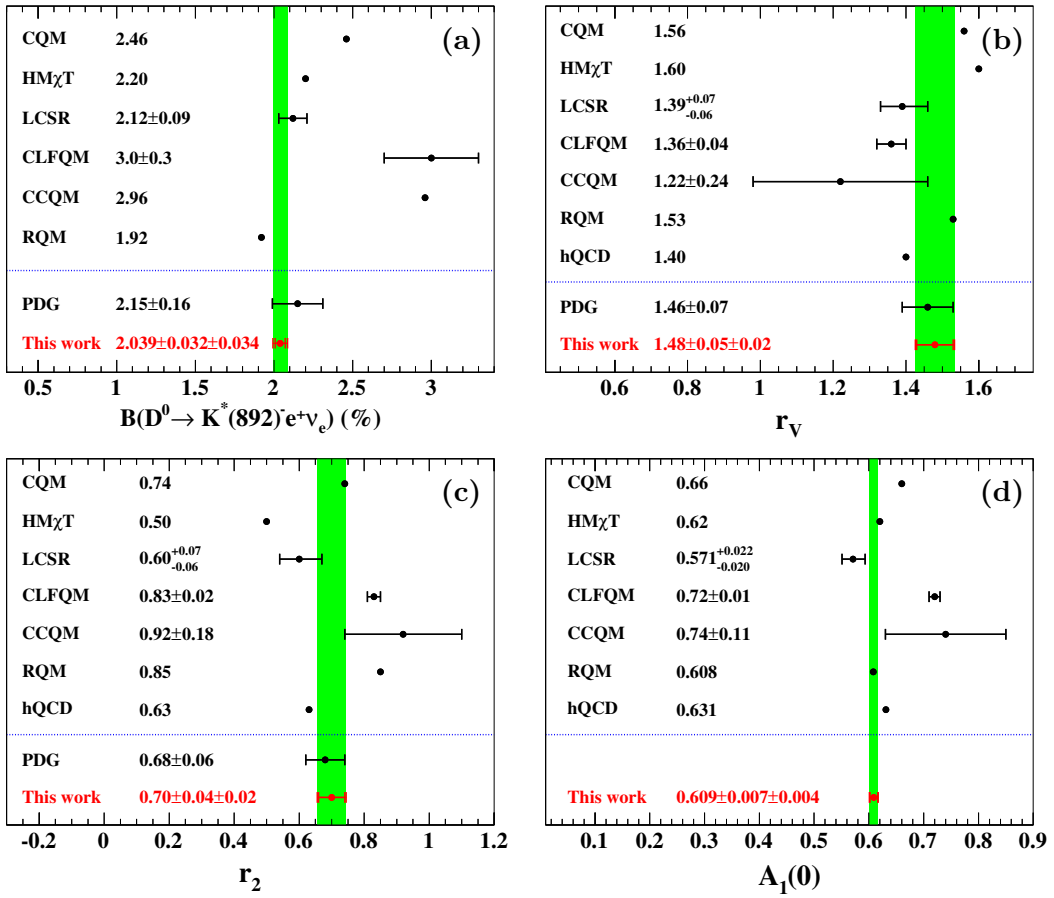


Figure 3. (Color online) Comparisons of the measured (a) $\mathcal{B}(D^0 \rightarrow K^*(892)^- e^+ \nu_e)$, (b) r_V , (c) r_2 and (d) $A_1(0)$ with various theoretical calculations from CQM [29], HM χ T [30], LCSR [31], CLFQM [32, 33], CCQM [34], RQM [35], hQCD [36] and PDG averaged results [21]. The inner (outer) error bars show the statistical (total) uncertainty.

The decay width of $D^0 \rightarrow K^*(892)^- e^+ \nu_e$ is related to $\mathcal{B}(D^0 \rightarrow K^*(892)^- e^+ \nu_e)$ measured in this work and the lifetime by

$$\Gamma = \frac{\hbar \mathcal{B}(D^0 \rightarrow K^*(892)^- e^+ \nu_e) \mathcal{B}(K^*(892)^- \rightarrow \bar{K}^0 \pi^-)}{\tau_{D^0}} = |A_1(0)|^2 |V_{cs}|^2 \times \mathbb{X}. \quad (6.2)$$

Here $\mathbb{X} = \frac{16}{9} \frac{G_F^2}{(4\pi)^5 m_{D^0}^2} \int_0^{q_{\max}^2} \int_{m_{\min}^2}^{m_{\max}^2} p_{\bar{K}^0 \pi} \beta \alpha^2 q^2 \times |\mathcal{A}(m)|^2 \frac{|H_0|^2 + |H_+|^2 + |H_-|^2}{|A_1(0)|^2} dm^2 dq^2$, where $q_{\max}^2 = (m_{D^0} - m_{\bar{K}^0} - m_\pi)^2$, and $m_{\bar{K}^0}$ and m_π are the known \bar{K}^0 and π^- masses [21]. The integration region over m^2 ranges from $m_{\min}^2 = (m_{\bar{K}^0} + m_\pi)^2$ to $m_{\max}^2 = 1.80^2 \text{ GeV}^2/c^4$. Then the integration in eq. (6.2) can be calculated using the form factor parameters measured in this work. Using the $\tau_{D^0} = 410.3 \pm 1.0 \text{ fs}$ and $|V_{cs}| = 0.97435 \pm 0.00016$ [21], we obtain $A_1(0) = 0.610 \pm 0.007 \pm 0.004$, which is the first determination using the data of $D^0 \rightarrow K^*(892)^- e^+ \nu_e$ decay. The comparisons of the $A_1(0)$ between this measurement and theoretical calculations are also shown in table 4 and figure 3.

Acknowledgments

The BESIII Collaboration thanks the staff of BEPCII and the IHEP computing center for their strong support. This work is supported in part by National Key R&D Program of China under Contracts Nos. 2023YFA1606000, 2020YFA0406300, 2020YFA0406400; National Natural Science Foundation of China (NSFC) under Contracts Nos. 11635010, 11735014, 11935015, 11935016, 11935018, 12022510, 12025502, 12035009, 12035013, 12061131003, 12192260, 12192261, 12192262, 12192263, 12192264, 12192265, 12221005, 12225509, 12235017, 12375090, 12361141819; the Chinese Academy of Sciences (CAS) Large-Scale Scientific Facility Program; the CAS Center for Excellence in Particle Physics (CCEPP); Joint Large-Scale Scientific Facility Funds of the NSFC and CAS under Contract No. U1832207; 100 Talents Program of CAS; The Institute of Nuclear and Particle Physics (INPAC) and Shanghai Key Laboratory for Particle Physics and Cosmology; German Research Foundation DFG under Contracts Nos. FOR5327, GRK 2149; Istituto Nazionale di Fisica Nucleare, Italy; Knut and Alice Wallenberg Foundation under Contracts Nos. 2021.0174, 2021.0299; Ministry of Development of Turkey under Contract No. DPT2006K-120470; National Research Foundation of Korea under Contract No. NRF-2022R1A2C1092335; National Science and Technology fund of Mongolia; National Science Research and Innovation Fund (NSRF) via the Program Management Unit for Human Resources & Institutional Development, Research and Innovation of Thailand under Contracts Nos. B16F640076, B50G670107; Polish National Science Centre under Contract No. 2019/35/O/ST2/02907; Swedish Research Council under Contract No. 2019.04595; The Swedish Foundation for International Cooperation in Research and Higher Education under Contract No. CH2018-7756; U. S. Department of Energy under Contract No. DE-FG02-05ER41374. This paper is also supported by the Fundamental Research Funds for the Central Universities, and the Research Funds of Renmin University of China under Contract No. 24XNKJ05.

Data Availability Statement. This article has no associated data or the data will not be deposited.

Code Availability Statement. This article has no associated code or the code will not be deposited.

Open Access. This article is distributed under the terms of the Creative Commons Attribution License ([CC-BY4.0](https://creativecommons.org/licenses/by/4.0/)), which permits any use, distribution and reproduction in any medium, provided the original author(s) and source are credited.

References

- [1] M. Antonelli et al., *Flavor Physics in the Quark Sector*, *Phys. Rept.* **494** (2010) 197 [[arXiv:0907.5386](https://arxiv.org/abs/0907.5386)] [[INSPIRE](#)].
- [2] N. Cabibbo, *Unitary Symmetry and Leptonic Decays*, *Phys. Rev. Lett.* **10** (1963) 531 [[INSPIRE](#)].
- [3] CLEO collaboration, *Model independent measurement of form-factors in the decay $D^+ \rightarrow K^- \pi^+ e^+ \nu_e$* , *Phys. Rev. D* **74** (2006) 052001 [[hep-ex/0606010](https://arxiv.org/abs/hep-ex/0606010)] [[INSPIRE](#)].
- [4] CLEO collaboration, *Analysis of and $D^+ \rightarrow K^- \pi^+ \mu^+ + \nu_\mu$ semileptonic decays*, *Phys. Rev. D* **81** (2006) 112001 [[arXiv:1004.1954](https://arxiv.org/abs/1004.1954)] [[INSPIRE](#)].
- [5] BABAR collaboration, *Analysis of the $D^+ \rightarrow K^- \pi^+ e^+ \nu_e$ decay channel*, *Phys. Rev. D* **83** (2011) 072001 [[arXiv:1012.1810](https://arxiv.org/abs/1012.1810)] [[INSPIRE](#)].
- [6] BESIII collaboration, *Study of $D^+ \rightarrow K^- \pi^+ e^+ \nu_e$* , *Phys. Rev. D* **94** (2016) 032001 [[arXiv:1512.08627](https://arxiv.org/abs/1512.08627)] [[INSPIRE](#)].
- [7] BESIII collaboration, *Study of the decay $D^0 \rightarrow \bar{K}^0 \pi^- e^+ \nu_e$* , *Phys. Rev. D* **99** (2019) 011103 [[arXiv:1811.11349](https://arxiv.org/abs/1811.11349)] [[INSPIRE](#)].
- [8] CLEO collaboration, *First Measurement of the Form Factors in the Decays $D^0 \rightarrow \rho^- e^+ \nu_e$ and $D^+ \rightarrow \rho^0 e^+ \nu_e$* , *Phys. Rev. Lett.* **110** (2013) 131802 [[arXiv:1112.2884](https://arxiv.org/abs/1112.2884)] [[INSPIRE](#)].
- [9] BESIII collaboration, *Measurement of the form factors in the decay $D^+ \rightarrow \omega e^+ \nu_e$ and search for the decay $D^+ \rightarrow \phi e^+ \nu_e$* , *Phys. Rev. D* **92** (2015) 071101 [[arXiv:1508.00151](https://arxiv.org/abs/1508.00151)] [[INSPIRE](#)].
- [10] BESIII collaboration, *Design and Construction of the BESIII Detector*, *Nucl. Instrum. Meth. A* **614** (2010) 345 [[arXiv:0911.4960](https://arxiv.org/abs/0911.4960)] [[INSPIRE](#)].
- [11] C. Yu et al., *BEPCII Performance and Beam Dynamics Studies on Luminosity*, in the proceedings of the *7th International Particle Accelerator Conference*, Busan, South Korea (2016) [[DOI:10.18429/JACoW-IPAC2016-TUYA01](https://doi.org/10.18429/JACoW-IPAC2016-TUYA01)] [[INSPIRE](#)].
- [12] BESIII collaboration, *Future Physics Programme of BESIII*, *Chin. Phys. C* **44** (2020) 040001 [[arXiv:1912.05983](https://arxiv.org/abs/1912.05983)] [[INSPIRE](#)].
- [13] X. Li et al., *Study of MRPC technology for BESIII endcap-TOF upgrade*, *Radiat. Detect. Technol. Methods* **1** (2017) 13 [[INSPIRE](#)].
- [14] Y.X. Guo et al., *The study of time calibration for upgraded end cap TOF of BESIII*, *Radiat. Detect. Technol. Meth.* **1** (2017) 15 [[INSPIRE](#)].
- [15] P. Cao et al., *Design and construction of the new BESIII endcap Time-of-Flight system with MRPC Technology*, *Nucl. Instrum. Meth. A* **953** (2020) 163053 [[INSPIRE](#)].
- [16] GEANT4 collaboration, *GEANT4 — A Simulation Toolkit*, *Nucl. Instrum. Meth. A* **506** (2003) 250 [[INSPIRE](#)].

- [17] S. Jadach, B.F.L. Ward and Z. Was, *The Precision Monte Carlo event generator KK for two fermion final states in e^+e^- collisions*, *Comput. Phys. Commun.* **130** (2000) 260 [[hep-ph/9912214](#)] [[INSPIRE](#)].
- [18] S. Jadach, B.F.L. Ward and Z. Was, *Coherent exclusive exponentiation for precision Monte Carlo calculations*, *Phys. Rev. D* **63** (2001) 113009 [[hep-ph/0006359](#)] [[INSPIRE](#)].
- [19] D.J. Lange, *The EvtGen particle decay simulation package*, *Nucl. Instrum. Meth. A* **462** (2001) 152 [[INSPIRE](#)].
- [20] R.G. Ping, *Event generators at BESIII*, *Chin. Phys. C* **32** (2008) 599 [[INSPIRE](#)].
- [21] PARTICLE DATA GROUP collaboration, *Review of particle physics*, *Phys. Rev. D* **110** (2024) 030001 [[INSPIRE](#)].
- [22] J.C. Chen et al., *Event generator for J/ψ and $\psi(2S)$ decay*, *Phys. Rev. D* **62** (2000) 034003 [[INSPIRE](#)].
- [23] E. Richter-Was, *QED bremsstrahlung in semileptonic B and leptonic tau decays*, *Phys. Lett. B* **303** (1993) 163 [[INSPIRE](#)].
- [24] ARGUS collaboration, *Search for Hadronic $b \rightarrow u$ Decays*, *Phys. Lett. B* **241** (1990) 278 [[INSPIRE](#)].
- [25] BESIII collaboration, *Study of decay dynamics and CP asymmetry in $D^+ \rightarrow K_L^0 e^+ \nu_e$ decay*, *Phys. Rev. D* **92** (2015) 112008 [[arXiv:1510.00308](#)] [[INSPIRE](#)].
- [26] BESIII collaboration, *Measurement of the Absolute Branching Fraction for $\Lambda_c^+ \rightarrow \Lambda \mu^+ \nu_\mu$* , *Phys. Rev. Lett.* **115** (2015) 221805 [[arXiv:1611.04382](#)] [[INSPIRE](#)].
- [27] C.L.Y. Lee, M. Lu and M.B. Wise, *$B(l_4)$ and $D(l_4)$ decay*, *Phys. Rev. D* **46** (1992) 5040 [[INSPIRE](#)].
- [28] J.D. Richman and P.R. Burchat, *Leptonic and semileptonic decays of charm and bottom hadrons*, *Rev. Mod. Phys.* **67** (1995) 893 [[hep-ph/9508250](#)] [[INSPIRE](#)].
- [29] D. Melikhov and B. Stech, *Weak form-factors for heavy meson decays: An Update*, *Phys. Rev. D* **62** (2000) 014006 [[hep-ph/0001113](#)] [[INSPIRE](#)].
- [30] S. Fajfer and J.F. Kamenik, *Charm meson resonances and $D \rightarrow V$ semileptonic form-factors*, *Phys. Rev. D* **72** (2005) 034029 [[hep-ph/0506051](#)] [[INSPIRE](#)].
- [31] Y.-L. Wu, M. Zhong and Y.-B. Zuo, *$B_{(s)}$, $D_{(s)} \rightarrow \pi, K, \eta, \rho, K^*, \omega, \phi$ Transition Form Factors and Decay Rates with Extraction of the CKM parameters $|V_{ub}|, |V_{cs}|, |V_{cd}|$* , *Int. J. Mod. Phys. A* **21** (2006) 6125 [[hep-ph/0604007](#)] [[INSPIRE](#)].
- [32] R.C. Verma, *Decay constants and form factors of s-wave and p-wave mesons in the covariant light-front quark model*, *J. Phys. G* **39** (2012) 025005 [[arXiv:1103.2973](#)] [[INSPIRE](#)].
- [33] H.-Y. Cheng and X.-W. Kang, *Branching fractions of semileptonic D and D_s decays from the covariant light-front quark model*, *Eur. Phys. J. C* **77** (2017) 587 [*Erratum ibid.* **77** (2017) 863] [[arXiv:1707.02851](#)] [[INSPIRE](#)].
- [34] M.A. Ivanov et al., *Exclusive semileptonic decays of D and D_s mesons in the covariant confining quark model*, *Front. Phys. (Beijing)* **14** (2019) 64401 [[arXiv:1904.07740](#)] [[INSPIRE](#)].
- [35] R.N. Faustov, V.O. Galkin and X.-W. Kang, *Semileptonic decays of D and D_s mesons in the relativistic quark model*, *Phys. Rev. D* **101** (2020) 013004 [[arXiv:1911.08209](#)] [[INSPIRE](#)].
- [36] H.A. Ahmed, Y. Chen and M. Huang, *$D(s)$ -mesons semileptonic form factors in four-flavor holographic QCD*, *Phys. Rev. D* **109** (2024) 026008 [[arXiv:2309.06156](#)] [[INSPIRE](#)].

The BESIII collaboration

M. Ablikim¹, M.N. Achasov^{4,c}, P. Adlarson⁷⁶, O. Afedulidis³, X.C. Ai⁸¹, R. Aliberti³⁵,
A. Amoroso^{75A,75C}, Y. Bai⁵⁷, O. Bakina³⁶, I. Balossino^{29A}, Y. Ban^{46,h}, H.-R. Bao⁶⁴,
V. Batozskaya^{1,44}, K. Begzsuren³², N. Berger³⁵, M. Berlowski⁴⁴, M. Bertani^{28A}, D. Bettoni^{29A},
F. Bianchi^{75A,75C}, E. Bianco^{75A,75C}, A. Bortone^{75A,75C}, I. Boyko³⁶, R.A. Briere⁵, A. Brueggemann⁶⁹,
H. Cai⁷⁷, X. Cai^{1,58}, A. Calcaterra^{28A}, G.F. Cao^{1,64}, N. Cao^{1,64}, S.A. Cetin^{62A}, X.Y. Chai^{46,h},
J.F. Chang^{1,58}, G.R. Che⁴³, Y.Z. Che^{1,58,64}, G. Chelkov^{36,b}, C. Chen⁴³, C.H. Chen⁹, Chao Chen⁵⁵,
G. Chen¹, H.S. Chen^{1,64}, H.Y. Chen²⁰, M.L. Chen^{1,58,64}, S.J. Chen⁴², S.L. Chen⁴⁵, S.M. Chen⁶¹,
T. Chen^{1,64}, X.R. Chen^{31,64}, X.T. Chen^{1,64}, Y.B. Chen^{1,58}, Y.Q. Chen³⁴, Z.J. Chen^{25,i}, S.K. Choi¹⁰,
G. Cibinetto^{29A}, F. Cossio^{75C}, J.J. Cui⁵⁰, H.L. Dai^{1,58}, J.P. Dai⁷⁹, A. Dbeyssi¹⁸, R. E. de Boer³,
D. Dedovich³⁶, C.Q. Deng⁷³, Z.Y. Deng¹, A. Denig³⁵, I. Denysenko³⁶, M. Destefanis^{75A,75C},
F. De Mori^{75A,75C}, B. Ding^{67,1}, X.X. Ding^{46,h}, Y. Ding⁴⁰, Y. Ding³⁴, J. Dong^{1,58}, L.Y. Dong^{1,64},
M.Y. Dong^{1,58,64}, X. Dong⁷⁷, M.C. Du¹, S.X. Du⁸¹, Y.Y. Duan⁵⁵, Z.H. Duan⁴², P. Egorov^{36,b},
G.F. Fan⁴², J.J. Fan¹⁹, Y.H. Fan⁴⁵, J. Fang^{1,58}, J. Fang⁵⁹, S.S. Fang^{1,64}, W.X. Fang¹, Y. Fang¹,
Y.Q. Fang^{1,58}, R. Farinelli^{29A}, L. Fava^{75B,75C}, F. Feldbauer³, G. Felici^{28A}, C.Q. Feng^{72,58},
J.H. Feng⁵⁹, Y.T. Feng^{72,58}, M. Fritsch³, C.D. Fu¹, J.L. Fu⁶⁴, Y.W. Fu^{1,64}, H. Gao⁶⁴, X.B. Gao⁴¹,
Y.N. Gao¹⁹, Y.N. Gao^{46,h}, Yang Gao^{72,58}, S. Garbolino^{75C}, I. Garzia^{29A,29B}, P.T. Ge¹⁹, Z.W. Ge⁴²,
C. Geng⁵⁹, E.M. Gersabeck⁶⁸, A. Gilman⁷⁰, K. Goetzen¹³, L. Gong⁴⁰, W.X. Gong^{1,58}, W. Gradl³⁵,
S. Gramigna^{29A,29B}, M. Greco^{75A,75C}, M.H. Gu^{1,58}, Y.T. Gu¹⁵, C.Y. Guan^{1,64}, A.Q. Guo^{31,64},
L.B. Guo⁴¹, M.J. Guo⁵⁰, R.P. Guo⁴⁹, Y.P. Guo^{12,g}, A. Guskov^{36,b}, J. Gutierrez²⁷, K.L. Han⁶⁴,
T.T. Han¹, F. Hanisch³, X.Q. Hao¹⁹, F.A. Harris⁶⁶, K.K. He⁵⁵, K.L. He^{1,64}, F.H. Heinsius³,
C.H. Heinz³⁵, Y.K. Heng^{1,58,64}, C. Herold⁶⁰, T. Holtmann³, P.C. Hong³⁴, G.Y. Hou^{1,64}, X.T. Hou^{1,64},
Y.R. Hou⁶⁴, Z.L. Hou¹, B.Y. Hu⁵⁹, H.M. Hu^{1,64}, J.F. Hu^{56,j}, Q.P. Hu^{72,58}, S.L. Hu^{12,g}, T. Hu^{1,58,64},
Y. Hu¹, G.S. Huang^{72,58}, K.X. Huang⁵⁹, L.Q. Huang^{31,64}, P. Huang⁴², X.T. Huang⁵⁰, Y.P. Huang¹,
Y.S. Huang⁵⁹, T. Hussain⁷⁴, F. Hölzken³, N. Hüskens³⁵, N. in der Wiesche⁶⁹, J. Jackson²⁷,
S. Janchiv³², Q. Ji¹, Q.P. Ji¹⁹, W. Ji^{1,64}, X.B. Ji^{1,64}, X.L. Ji^{1,58}, Y.Y. Ji⁵⁰, X.Q. Jia⁵⁰, Z.K. Jia^{72,58},
D. Jiang^{1,64}, H.B. Jiang⁷⁷, P.C. Jiang^{46,h}, S.S. Jiang³⁹, T.J. Jiang¹⁶, X.S. Jiang^{1,58,64}, Y. Jiang⁶⁴,
J.B. Jiao⁵⁰, J.K. Jiao³⁴, Z. Jiao²³, S. Jin⁴², Y. Jin⁶⁷, M.Q. Jing^{1,64}, X.M. Jing⁶⁴, T. Johansson⁷⁶,
S. Kabana³³, N. Kalantar-Nayestanaki⁶⁵, X.L. Kang⁹, X.S. Kang⁴⁰, M. Kavatsyuk⁶⁵, B.C. Ke⁸¹,
V. Khachatryan²⁷, A. Khoukaz⁶⁹, R. Kiuchi¹, O.B. Kolcu^{62A}, B. Kopf³, M. Kuessner³, X. Kui^{1,64},
N. Kumar²⁶, A. Kupsc^{44,76}, W. Kühn³⁷, W.N. Lan¹⁹, T.T. Lei^{72,58}, Z.H. Lei^{72,58}, M. Lellmann³⁵,
T. Lenz³⁵, C. Li⁴³, C. Li⁴⁷, C.H. Li³⁹, Cheng Li^{72,58}, D.M. Li⁸¹, F. Li^{1,58}, G. Li¹, H.B. Li^{1,64},
H.J. Li¹⁹, H.N. Li^{56,j}, Hui Li⁴³, J.R. Li⁶¹, J.S. Li⁵⁹, K. Li¹, K.L. Li¹⁹, L.J. Li^{1,64}, L.K. Li¹, Lei Li⁴⁸,
M.H. Li⁴³, P.L. Li⁶⁴, P.R. Li^{38,k,l}, Q.M. Li^{1,64}, Q.X. Li⁵⁰, R. Li^{17,31}, T. Li⁵⁰, T.Y. Li⁴³, W.D. Li^{1,64},
W.G. Li^{1,a}, X. Li^{1,64}, X.H. Li^{72,58}, X.L. Li⁵⁰, X.Y. Li^{1,8}, X.Z. Li⁵⁹, Y. Li¹⁹, Y.G. Li^{46,h}, Z.J. Li⁵⁹,
Z.Y. Li⁷⁹, C. Liang⁴², H. Liang^{1,64}, H. Liang^{72,58}, Y.F. Liang⁵⁴, Y.T. Liang^{31,64}, G.R. Liao¹⁴,
Y.P. Liao^{1,64}, J. Libby²⁶, A. Limphirat⁶⁰, C.C. Lin⁵⁵, C.X. Lin⁶⁴, D.X. Lin^{31,64}, T. Lin¹, B.J. Liu¹,
B.X. Liu⁷⁷, C. Liu³⁴, C.X. Liu¹, F. Liu¹, F.H. Liu⁵³, Feng Liu⁶, G.M. Liu^{56,j}, H. Liu^{38,k,l}, H.B. Liu¹⁵,
H.H. Liu¹, H.M. Liu^{1,64}, Huihui Liu²¹, J.B. Liu^{72,58}, J.Y. Liu^{1,64}, K. Liu^{38,k,l}, K.Y. Liu⁴⁰, Ke Liu²²,
L. Liu^{72,58}, L.C. Liu⁴³, Lu Liu⁴³, M.H. Liu^{12,g}, P.L. Liu¹, Q. Liu⁶⁴, S.B. Liu^{72,58}, T. Liu^{12,g},
W.K. Liu⁴³, W.M. Liu^{72,58}, X. Liu^{38,k,l}, X. Liu³⁹, Y. Liu^{38,k,l}, Y. Liu⁸¹, Y.B. Liu⁴³, Z.A. Liu^{1,58,64},
Z.D. Liu⁹, Z.Q. Liu⁵⁰, X.C. Lou^{1,58,64}, F.X. Lu⁵⁹, H.J. Lu²³, J.G. Lu^{1,58}, Y. Lu⁷, Y.P. Lu^{1,58},
Z.H. Lu^{1,64}, C.L. Luo⁴¹, J.R. Luo⁵⁹, M.X. Luo⁸⁰, T. Luo^{12,g}, X.L. Luo^{1,58}, X.R. Lyu⁶⁴, Y.F. Lyu⁴³,

F.C. Ma⁴⁰, H. Ma⁷⁹, H.L. Ma¹, J.L. Ma^{1,64}, L.L. Ma⁵⁰, L.R. Ma⁶⁷, M.M. Ma^{1,64}, Q.M. Ma¹,
 R.Q. Ma^{1,64}, R.Y. Ma¹⁹, T. Ma^{72,58}, X.T. Ma^{1,64}, X.Y. Ma^{1,58}, Y.M. Ma³¹, F.E. Maas¹⁸,
 I. MacKay⁷⁰, M. Maggiora^{75A,75C}, S. Malde⁷⁰, Y.J. Mao^{46,h}, Z.P. Mao¹, S. Marcello^{75A,75C},
 Y.H. Meng⁶⁴, Z.X. Meng⁶⁷, J.G. Messchendorp^{13,65}, G. Mezzadri^{29A}, H. Miao^{1,64}, T.J. Min⁴²,
 R.E. Mitchell²⁷, X.H. Mo^{1,58,64}, B. Moses²⁷, N. Yu. Muchnoi^{4,c}, J. Muskalla³⁵, Y. Nefedov³⁶,
 F. Nerling^{18,e}, L.S. Nie²⁰, I.B. Nikolaev^{4,c}, Z. Ning^{1,58}, S. Nisar^{11,m}, Q.L. Niu^{38,k,l}, W.D. Niu⁵⁵,
 Y. Niu⁵⁰, S.L. Olsen^{10,64}, Q. Ouyang^{1,58,64}, S. Pacetti^{28B,28C}, X. Pan⁵⁵, Y. Pan⁵⁷, A. Pathak¹⁰,
 Y.P. Pei^{72,58}, M. Pelizaesus³, H.P. Peng^{72,58}, Y.Y. Peng^{38,k,l}, K. Peters^{13,e}, J.L. Ping⁴¹, R.G. Ping^{1,64},
 S. Plura³⁵, V. Prasad³³, F.Z. Qi¹, H. Qi^{72,58}, H.R. Qi⁶¹, M. Qi⁴², S. Qian^{1,58}, W.B. Qian⁶⁴,
 C.F. Qiao⁶⁴, J.H. Qiao¹⁹, J.J. Qin⁷³, L.Q. Qin¹⁴, L.Y. Qin^{72,58}, X.P. Qin^{12,g}, X.S. Qin⁵⁰, Z.H. Qin^{1,58},
 J.F. Qiu¹, Z.H. Qu⁷³, C.F. Redmer³⁵, K.J. Ren³⁹, A. Rivetti^{75C}, M. Rolo^{75C}, G. Rong^{1,64},
 Ch. Rosner¹⁸, M.Q. Ruan^{1,58}, S.N. Ruan⁴³, N. Salone⁴⁴, A. Sarantsev^{36,d}, Y. Schelhaas³⁵,
 K. Schoenning⁷⁶, M. Scodeggio^{29A}, K.Y. Shan^{12,g}, W. Shan²⁴, X.Y. Shan^{72,58}, Z.J. Shang^{38,k,l},
 J.F. Shangguan¹⁶, L.G. Shao^{1,64}, M. Shao^{72,58}, C.P. Shen^{12,g}, H.F. Shen^{1,8}, W.H. Shen⁶⁴,
 X.Y. Shen^{1,64}, B.A. Shi⁶⁴, H. Shi^{72,58}, J.L. Shi^{12,g}, J.Y. Shi¹, S.Y. Shi⁷³, X. Shi^{1,58}, J.J. Song¹⁹,
 T.Z. Song⁵⁹, W.M. Song^{34,1}, Y. J. Song^{12,g}, Y.X. Song^{46,h,n}, S. Sosio^{75A,75C}, S. Spataro^{75A,75C},
 F. Stielor³⁵, S. S. Su⁴⁰, Y.J. Su⁶⁴, G.B. Sun⁷⁷, G.X. Sun¹, H. Sun⁶⁴, H.K. Sun¹, J.F. Sun¹⁹, K. Sun⁶¹,
 L. Sun⁷⁷, S.S. Sun^{1,64}, T. Sun^{51,f}, Y.J. Sun^{72,58}, Y.Z. Sun¹, Z.Q. Sun^{1,64}, Z.T. Sun⁵⁰, C.J. Tang⁵⁴,
 G.Y. Tang¹, J. Tang⁵⁹, M. Tang^{72,58}, Y.A. Tang⁷⁷, L.Y. Tao⁷³, M. Tat⁷⁰, J.X. Teng^{72,58},
 V. Thoren⁷⁶, W.H. Tian⁵⁹, Y. Tian^{31,64}, Z.F. Tian⁷⁷, I. Uman^{62B}, Y. Wan⁵⁵, S.J. Wang⁵⁰, B. Wang¹,
 Bo Wang^{72,58}, C. Wang¹⁹, D.Y. Wang^{46,h}, H.J. Wang^{38,k,l}, J.J. Wang⁷⁷, J.P. Wang⁵⁰, K. Wang^{1,58},
 L.L. Wang¹, L.W. Wang³⁴, M. Wang⁵⁰, N.Y. Wang⁶⁴, S. Wang^{12,g}, S. Wang^{38,k,l}, T. Wang^{12,g},
 T.J. Wang⁴³, W. Wang⁷³, W. Wang⁵⁹, W.P. Wang^{35,58,72,o}, X. Wang^{46,h}, X.F. Wang^{38,k,l},
 X.J. Wang³⁹, X.L. Wang^{12,g}, X.N. Wang¹, Y. Wang⁶¹, Y.D. Wang⁴⁵, Y.F. Wang^{1,58,64},
 Y.H. Wang^{38,k,l}, Y.L. Wang¹⁹, Y.N. Wang⁴⁵, Y.Q. Wang¹, Yaqian Wang¹⁷, Yi Wang⁶¹, Z. Wang^{1,58},
 Z.L. Wang⁷³, Z.Y. Wang^{1,64}, D.H. Wei¹⁴, F. Weidner⁶⁹, S.P. Wen¹, Y.R. Wen³⁹, U. Wiedner³,
 G. Wilkinson⁷⁰, M. Wolke⁷⁶, L. Wollenberg³, C. Wu³⁹, J.F. Wu^{1,8}, L.H. Wu¹, L.J. Wu^{1,64},
 Lianjie Wu¹⁹, X. Wu^{12,g}, X.H. Wu³⁴, Y.H. Wu⁵⁵, Y.J. Wu³¹, Z. Wu^{1,58}, L. Xia^{72,58}, X.M. Xian³⁹,
 B.H. Xiang^{1,64}, T. Xiang^{46,h}, D. Xiao^{38,k,l}, G.Y. Xiao⁴², H. Xiao⁷³, S.Y. Xiao¹, Y.L. Xiao^{12,g},
 Z.J. Xiao⁴¹, C. Xie⁴², X.H. Xie^{46,h}, Y. Xie⁵⁰, Y.G. Xie^{1,58}, Y.H. Xie⁶, Z.P. Xie^{72,58}, T.Y. Xing^{1,64},
 C.F. Xu^{1,64}, C.J. Xu⁵⁹, G.F. Xu¹, M. Xu^{72,58}, Q.J. Xu¹⁶, Q.N. Xu³⁰, W.L. Xu⁶⁷, X.P. Xu⁵⁵, Y. Xu⁴⁰,
 Y.C. Xu⁷⁸, Z.S. Xu⁶⁴, F. Yan^{12,g}, L. Yan^{12,g}, W.B. Yan^{72,58}, W.C. Yan⁸¹, W.P. Yan¹⁹, X.Q. Yan^{1,64},
 H.J. Yang^{51,f}, H.L. Yang³⁴, H.X. Yang¹, J.H. Yang⁴², R.J. Yang¹⁹, T. Yang¹, Y. Yang^{12,g},
 Y.F. Yang⁴³, Y.F. Yang^{1,64}, Y.X. Yang^{1,64}, Y.Z. Yang¹⁹, Z.W. Yang^{38,k,l}, Z.P. Yao⁵⁰, M. Ye^{1,58},
 M.H. Ye⁸, J.H. Yin¹, Junhao Yin⁴³, Z.Y. You⁵⁹, B.X. Yu^{1,58,64}, C.X. Yu⁴³, G. Yu^{1,64}, J.S. Yu^{25,i},
 M.C. Yu⁴⁰, T. Yu⁷³, X.D. Yu^{46,h}, C.Z. Yuan^{1,64}, J. Yuan³⁴, J. Yuan⁴⁵, L. Yuan², S.C. Yuan^{1,64},
 Y. Yuan^{1,64}, Z.Y. Yuan⁵⁹, C.X. Yue³⁹, Ying Yue¹⁹, A.A. Zafar⁷⁴, F.R. Zeng⁵⁰, S.H. Zeng⁶³,
 X. Zeng^{12,g}, Y. Zeng^{25,i}, Y.J. Zeng⁵⁹, Y.J. Zeng^{1,64}, X.Y. Zhai³⁴, Y.C. Zhai⁵⁰, Y.H. Zhan⁵⁹,
 A.Q. Zhang^{1,64}, B.L. Zhang^{1,64}, B.X. Zhang¹, D.H. Zhang⁴³, G.Y. Zhang¹⁹, H. Zhang⁸¹,
 H. Zhang^{72,58}, H.C. Zhang^{1,58,64}, H.H. Zhang⁵⁹, H.Q. Zhang^{1,58,64}, H.R. Zhang^{72,58}, H.Y. Zhang^{1,58},
 J. Zhang⁵⁹, J. Zhang⁸¹, J.J. Zhang⁵², J.L. Zhang²⁰, J.Q. Zhang⁴¹, J.S. Zhang^{12,g}, J.W. Zhang^{1,58,64},
 J.X. Zhang^{38,k,l}, J.Y. Zhang¹, J.Z. Zhang^{1,64}, Jianyu Zhang⁶⁴, L.M. Zhang⁶¹, Lei Zhang⁴²,
 P. Zhang^{1,64}, Q. Zhang¹⁹, Q.Y. Zhang³⁴, R.Y. Zhang^{38,k,l}, S.H. Zhang^{1,64}, Shulei Zhang^{25,i},

X.M. Zhang¹, X. Y Zhang⁴⁰, X.Y. Zhang⁵⁰, Y. Zhang⁷³, Y. Zhang¹, Y.T. Zhang⁸¹, Y.H. Zhang^{1,58}, Y.M. Zhang³⁹, Yan Zhang^{72,58}, Z.D. Zhang¹, Z.H. Zhang¹, Z.L. Zhang³⁴, Z.X. Zhang¹⁹, Z.Y. Zhang⁴³, Z.Y. Zhang⁷⁷, Z.Z. Zhang⁴⁵, Zh. Zh. Zhang¹⁹, G. Zhao¹, J.Y. Zhao^{1,64}, J.Z. Zhao^{1,58}, L. Zhao¹, Lei Zhao^{72,58}, M.G. Zhao⁴³, N. Zhao⁷⁹, R.P. Zhao⁶⁴, S.J. Zhao⁸¹, Y.B. Zhao^{1,58}, Y.X. Zhao^{31,64}, Z.G. Zhao^{72,58}, A. Zhemchugov^{36,b}, B. Zheng⁷³, B.M. Zheng³⁴, J.P. Zheng^{1,58}, W.J. Zheng^{1,64}, X.R. Zheng¹⁹, Y.H. Zheng⁶⁴, B. Zhong⁴¹, X. Zhong⁵⁹, H. Zhou^{35,50,o}, J.Y. Zhou³⁴, L.P. Zhou^{1,64}, S. Zhou⁶, X. Zhou⁷⁷, X.K. Zhou⁶, X.R. Zhou^{72,58}, X.Y. Zhou³⁹, Y.Z. Zhou^{12,g}, Z.C. Zhou²⁰, A.N. Zhu⁶⁴, J. Zhu⁴³, K. Zhu¹, K.J. Zhu^{1,58,64}, K.S. Zhu^{12,g}, L. Zhu³⁴, L.X. Zhu⁶⁴, S.H. Zhu⁷¹, T.J. Zhu^{12,g}, W.D. Zhu⁴¹, W.Z. Zhu¹⁹, Y.C. Zhu^{72,58}, Z.A. Zhu^{1,64}, J.H. Zou¹, J. Zu^{72,58}

¹ *Institute of High Energy Physics, Beijing 100049, People's Republic of China*

² *Beihang University, Beijing 100191, People's Republic of China*

³ *Bochum Ruhr-University, D-44780 Bochum, Germany*

⁴ *Budker Institute of Nuclear Physics SB RAS (BINP), Novosibirsk 630090, Russia*

⁵ *Carnegie Mellon University, Pittsburgh, Pennsylvania 15213, USA*

⁶ *Central China Normal University, Wuhan 430079, People's Republic of China*

⁷ *Central South University, Changsha 410083, People's Republic of China*

⁸ *China Center of Advanced Science and Technology, Beijing 100190, People's Republic of China*

⁹ *China University of Geosciences, Wuhan 430074, People's Republic of China*

¹⁰ *Chung-Ang University, Seoul, 06974, Republic of Korea*

¹¹ *COMSATS University Islamabad, Lahore Campus, Defence Road, Off Raiwind Road, 54000 Lahore, Pakistan*

¹² *Fudan University, Shanghai 200433, People's Republic of China*

¹³ *GSI Helmholtzcentre for Heavy Ion Research GmbH, D-64291 Darmstadt, Germany*

¹⁴ *Guangxi Normal University, Guilin 541004, People's Republic of China*

¹⁵ *Guangxi University, Nanning 530004, People's Republic of China*

¹⁶ *Hangzhou Normal University, Hangzhou 310036, People's Republic of China*

¹⁷ *Hebei University, Baoding 071002, People's Republic of China*

¹⁸ *Helmholtz Institute Mainz, Staudinger Weg 18, D-55099 Mainz, Germany*

¹⁹ *Henan Normal University, Xinxiang 453007, People's Republic of China*

²⁰ *Henan University, Kaifeng 475004, People's Republic of China*

²¹ *Henan University of Science and Technology, Luoyang 471003, People's Republic of China*

²² *Henan University of Technology, Zhengzhou 450001, People's Republic of China*

²³ *Huangshan College, Huangshan 245000, People's Republic of China*

²⁴ *Hunan Normal University, Changsha 410081, People's Republic of China*

²⁵ *Hunan University, Changsha 410082, People's Republic of China*

²⁶ *Indian Institute of Technology Madras, Chennai 600036, India*

²⁷ *Indiana University, Bloomington, Indiana 47405, USA*

²⁸ *INFN Laboratori Nazionali di Frascati, (A)INFN Laboratori Nazionali di Frascati, I-00044, Frascati, Italy; (B)INFN Sezione di Perugia, I-06100, Perugia, Italy; (C)University of Perugia, I-06100, Perugia, Italy*

²⁹ *INFN Sezione di Ferrara, (A)INFN Sezione di Ferrara, I-44122, Ferrara, Italy; (B)University of Ferrara, I-44122, Ferrara, Italy*

³⁰ *Inner Mongolia University, Hohhot 010021, People's Republic of China*

³¹ *Institute of Modern Physics, Lanzhou 730000, People's Republic of China*

³² *Institute of Physics and Technology, Peace Avenue 54B, Ulaanbaatar 13330, Mongolia*

³³ *Instituto de Alta Investigación, Universidad de Tarapacá, Casilla 7D, Arica 1000000, Chile*

³⁴ *Jilin University, Changchun 130012, People's Republic of China*

³⁵ *Johannes Gutenberg University of Mainz, Johann-Joachim-Becher-Weg 45, D-55099 Mainz, Germany*

³⁶ *Joint Institute for Nuclear Research, 141980 Dubna, Moscow region, Russia*

³⁷ *Justus-Liebig-Universität Giessen, II. Physikalisches Institut, Heinrich-Buff-Ring 16, D-35392 Giessen, Germany*

- ³⁸ Lanzhou University, Lanzhou 730000, People's Republic of China
- ³⁹ Liaoning Normal University, Dalian 116029, People's Republic of China
- ⁴⁰ Liaoning University, Shenyang 110036, People's Republic of China
- ⁴¹ Nanjing Normal University, Nanjing 210023, People's Republic of China
- ⁴² Nanjing University, Nanjing 210093, People's Republic of China
- ⁴³ Nankai University, Tianjin 300071, People's Republic of China
- ⁴⁴ National Centre for Nuclear Research, Warsaw 02-093, Poland
- ⁴⁵ North China Electric Power University, Beijing 102206, People's Republic of China
- ⁴⁶ Peking University, Beijing 100871, People's Republic of China
- ⁴⁷ Qufu Normal University, Qufu 273165, People's Republic of China
- ⁴⁸ Renmin University of China, Beijing 100872, People's Republic of China
- ⁴⁹ Shandong Normal University, Jinan 250014, People's Republic of China
- ⁵⁰ Shandong University, Jinan 250100, People's Republic of China
- ⁵¹ Shanghai Jiao Tong University, Shanghai 200240, People's Republic of China
- ⁵² Shanxi Normal University, Linfen 041004, People's Republic of China
- ⁵³ Shanxi University, Taiyuan 030006, People's Republic of China
- ⁵⁴ Sichuan University, Chengdu 610064, People's Republic of China
- ⁵⁵ Soochow University, Suzhou 215006, People's Republic of China
- ⁵⁶ South China Normal University, Guangzhou 510006, People's Republic of China
- ⁵⁷ Southeast University, Nanjing 211100, People's Republic of China
- ⁵⁸ State Key Laboratory of Particle Detection and Electronics, Beijing 100049, Hefei 230026, People's Republic of China
- ⁵⁹ Sun Yat-Sen University, Guangzhou 510275, People's Republic of China
- ⁶⁰ Suranaree University of Technology, University Avenue 111, Nakhon Ratchasima 30000, Thailand
- ⁶¹ Tsinghua University, Beijing 100084, People's Republic of China
- ⁶² Turkish Accelerator Center Particle Factory Group, (A)Istinye University, 34010, Istanbul, Turkey; (B)Near East University, Nicosia, North Cyprus, 99138, Mersin 10, Turkey
- ⁶³ University of Bristol, H H Wills Physics Laboratory, Tyndall Avenue, Bristol, BS8 1TL, UK
- ⁶⁴ University of Chinese Academy of Sciences, Beijing 100049, People's Republic of China
- ⁶⁵ University of Groningen, NL-9747 AA Groningen, The Netherlands
- ⁶⁶ University of Hawaii, Honolulu, Hawaii 96822, USA
- ⁶⁷ University of Jinan, Jinan 250022, People's Republic of China
- ⁶⁸ University of Manchester, Oxford Road, Manchester, M13 9PL, United Kingdom
- ⁶⁹ University of Muenster, Wilhelm-Klemm-Strasse 9, 48149 Muenster, Germany
- ⁷⁰ University of Oxford, Keble Road, Oxford OX13RH, United Kingdom
- ⁷¹ University of Science and Technology Liaoning, Anshan 114051, People's Republic of China
- ⁷² University of Science and Technology of China, Hefei 230026, People's Republic of China
- ⁷³ University of South China, Hengyang 421001, People's Republic of China
- ⁷⁴ University of the Punjab, Lahore-54590, Pakistan
- ⁷⁵ University of Turin and INFN, (A)University of Turin, I-10125, Turin, Italy; (B)University of Eastern Piedmont, I-15121, Alessandria, Italy; (C)INFN, I-10125, Turin, Italy
- ⁷⁶ Uppsala University, Box 516, SE-75120 Uppsala, Sweden
- ⁷⁷ Wuhan University, Wuhan 430072, People's Republic of China
- ⁷⁸ Yantai University, Yantai 264005, People's Republic of China
- ⁷⁹ Yunnan University, Kunming 650500, People's Republic of China
- ⁸⁰ Zhejiang University, Hangzhou 310027, People's Republic of China
- ⁸¹ Zhengzhou University, Zhengzhou 450001, People's Republic of China

^a Deceased

^b Also at the Moscow Institute of Physics and Technology, Moscow 141700, Russia

^c Also at the Novosibirsk State University, Novosibirsk, 630090, Russia

^d Also at the NRC "Kurchatov Institute", PNPI, 188300, Gatchina, Russia

^e Also at Goethe University Frankfurt, 60323 Frankfurt am Main, Germany

^f Also at Key Laboratory for Particle Physics, Astrophysics and Cosmology, Ministry of Education; Shanghai Key Laboratory for Particle Physics and Cosmology; Institute of Nuclear and Particle Physics, Shanghai 200240, People's Republic of China

^g Also at Key Laboratory of Nuclear Physics and Ion-beam Application (MOE) and Institute of Modern Physics, Fudan University, Shanghai 200443, People's Republic of China

^h Also at State Key Laboratory of Nuclear Physics and Technology, Peking University, Beijing 100871, People's Republic of China

ⁱ Also at School of Physics and Electronics, Hunan University, Changsha 410082, China

^j Also at Guangdong Provincial Key Laboratory of Nuclear Science, Institute of Quantum Matter, South China Normal University, Guangzhou 510006, China

^k Also at MOE Frontiers Science Center for Rare Isotopes, Lanzhou University, Lanzhou 730000, People's Republic of China

^l Also at Lanzhou Center for Theoretical Physics, Lanzhou University, Lanzhou 730000, People's Republic of China

^m Also at the Department of Mathematical Sciences, IBA, Karachi 75270, Pakistan

ⁿ Also at Ecole Polytechnique Federale de Lausanne (EPFL), CH-1015 Lausanne, Switzerland

^o Also at Helmholtz Institute Mainz, Staudinger Weg 18, D-55099 Mainz, Germany